CERN - European Laboratory for Particle Physics

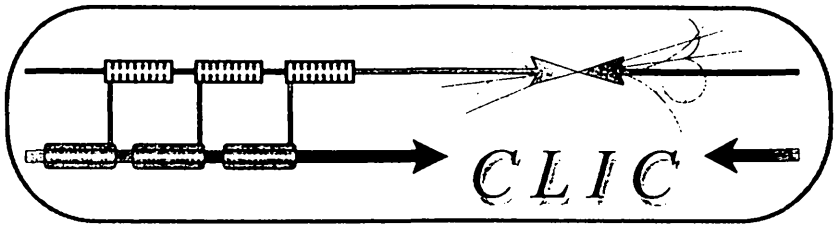

CLIC Note 409

PS/RF Note 99-04

Beam Dynamics in the Accelerating RF Structures of the CTF2 Drive Beam Simulated with PARMELA Particle Tracking Program

M. CHANUDET
CERN PS/RF

Abstract

The behavior of the CTF2 drive beam is studied through the first elements of the line for a bunch train of 48×10nC. Simulations were realised with the PARMELA program which tracks particles through different RF and magnetic elements. Space charge and beam loading in RF structures are included in the calculations, but not the wakefields. In this note, all the beam, RF and magnetic parameters are chosen to approach the operational settings of the CTF2 at the end of 98 and the beginning of 99. Two configurations are reported and compared. The first is chosen to describe the Nov. 98 experimental layout. The second one with a booster section is proposed to improve the beam characteristics.

The PARMELA beam generation is discussed. Then, the fields in the HCS sections are studied, a purely standing wave in the couplers is put in evidence and a model of the HCS is deduced and tested for the PARMELA simulations. The RF effects of the HCS section on the beam dynamics are demonstrated, in particular the critical focusing of the input HCS1 coupler. The simulations of the two layouts focus also on train transmission, beam envelopes and energy spreads inside the bunches and over the train.

Geneva, Switzerland
25 July 1999

Beam dynamics in the accelerating RF structures of the CTF2 drive beam simulated with PARMELA particle tracking program

M. CHANUDET
CERN PS/RF

I. Introduction

The behavior of the CTF2 drive beam [1] is studied only through the accelerating RF structures of the line. The purpose is to get a better knowledge of the influence of the RF forces on the beam transport and particularly on the transverse dynamics in the HCS accelerating structures. Simulations were realised with the PARMELA program which tracks particles through different RF and magnetic elements in the cartesian coordinates. (The version 4.22 available from LAL [2] was used on UNIX cluster.) All the beam, RF and magnetic parameters are chosen to approach the operational settings of the CTF2 in 98 and near future (99). Two configurations are reported (see figure 9 and table 2). The first is chosen to describe the Nov 98 experimental layout. In the second one, the second solenoid is replaced by a two cell structure called booster to focuse and accelerate the beam. And a five cell structure called buncher is added after the HCS structures to introduce correlation and more energy gain in the bunches. By this new proposition, improvements of the beam characteristics can be predicted. The CTF2 drive beam is constituted by 48 bunches of 10nC each, with a bunch length of 8ps fwhm and a bunch repetition rate of 2998.55MHz. The average accelerating gradients in the booster, HCS structures and buncher are of 35MV/m. Space charge and beam loading in RF structures are included in the calculations but not the wakefield.

First, the inputs used in PARMELA simulations are introduced. The particle distribution at the output of the gun is presented and discussed. The fields in the HCS sections are studied, particularly the fringe fields and standing waves in the couplers. A model of the HCS is deduced and tested for the PARMELA simulations. The data for the other RF and magnetic elements are presented and commented. Then, the two different runs are presented and compared. The influence of the RF forces and some particularities of the transmission are explained.

II. Beam representation at the input of the simulated lines

The PARMELA program generates macro-particles of a bunch in the phase space and then tracks them trough the different elements. Each bunch is simulated separately, but only the 1st, 24th and 48th bunches are calculated here because of their order and extreme energies in the train. The object of this paragraph is to precise the main beam characteristics at the input and then to explain how they are transposed in PARMELA input description.

The gun4 and solenoid 1 were simulated by M. Dehler with MAFIA code for the case of a laser spot of 16mm diameter, a laser phase of 30°, a gun field of 100MV/m and 48 bunches of 21nC each [3]. In this paper, we use the CTF2 Nov 98 settings which involve only a laser spot of about 11mm and bunches of 10nC. As in this two cases, the charge density on the cathode is the same with 10.5nC/cm^2, the dominating space charge force in the gun is kept constant and the transverse sizes of the bunches can be linearly extrapolated to the new settings. Furthermore, the emittance varies linearly with the bunch charge and thus it must be scaled here by the factor 10nC/21nC.

In PARMELA, the particles are generated in the transverse phase spaces (x, x') and (y, y') with a gaussian distribution in the phase space ellipses (see figures 1.a, b, c). The cartesian coordonates (x, y) are used rather than the cylindrical coordinates (r, θ) with MAFIA. To put the emphasis on the transmission of the external particles rather than the rms values, the same maxima are used between polar and cartesian description. We have here $r_{max}=x_{max}=y_{max}$ and $r'_{max}=x'_{max}=y'_{max}$.

In the longitudinal phase space (z, E_{kin}), the PARMELA particles are distributed uniformly in a phase space ellipse (see figure 1.d) rather than in a square to avoid unrealistic particles with too high divergence. The same rms values as in MAFIA code are used with z_{rms}=1mm and $\Delta\gamma_{rms}/\gamma$ from 1.3% to 1.7%.

Finally, for the Nov 98 configuration, the PARMELA run begins before solenoid 1 so that the magnetic field of the solenoid can be easier adjusted. The source of particles has been located on a virtual cathode 100mm in front of the solenoid 1 outside of the magnetic field, in order to avoid any emittance blow-up at the source. The beam characteristics at the virtual cathode were chosen so as to reproduce the MAFIA results obtained for gun 4 at the exit of the solenoid 1. For the booster configuration, the PARMELA run begins only at 50mm from the exit of solenoid 1 with MAFIA results. The table 1 recapitulates the input beam data used for the two PARMELA simulations reported in this note.

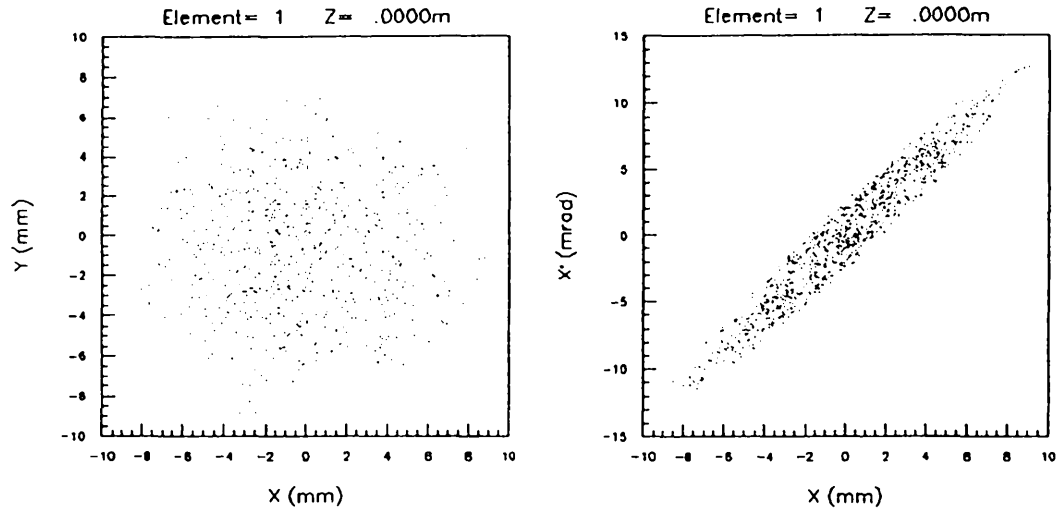

(a) Real transverse plan (x, y) **(b) Horizontal transverse phase space (x, x')**

(c) Vertical transverse phase space (y, y') **(d) Longitudinal phase space (Φ, E_{kin})**

Figure 1: *Distribution of the macro-particles generated at the PARMELA input for the first bunch at 50mm of the exit of solenoid 1.*

		Booster run Exit of solenoid 1			Nov 98 run Virtual cathode		
bunch n°		**1**	**24**	**48**	**1**	**24**	**48**
$x_{max}=y_{max}$	**mm**	9.21	9.56	9.83	3.85	3.99	4.14
$x'_{max}=y'_{max}$	**mrad**	13.27	11.83	10.11	26.74	28.14	30.38
$\varepsilon_x=\varepsilon_y$	**mm.mrad**	60.	62.	64.	48.	49.	51.
Δz_{rms}	**mm**	0.99	1.02	1.05	0.99	1.02	1.05
γ		14.0	13.1	12.1	14.0	13.1	12.1
$\Delta\gamma_{rms}/\gamma$	%	1.3	1.5	1.7	1.3	1.5	1.7

Table 1: *Input beam characteristics for the two simulated lines.*

III. Description of the HCS travelling wave structures

Once the beam input is given, the description of the different elements of the line must be done in PARMELA. In this part, the complex HCS sections (High Charge Structure) [4] are studied to determine a realistic PARMELA model. These structures are travelling wave sections operating on a phase advance of $11\pi/12$ per cell. They are constituted of input and output couplers with 13 cavities between. Their frequencies are different from the bunch frequency with 3006.36MHz for HCS1 and 2998.74MHz for HCS2. Their asynchronous operation and the choice of their RF phase allow to decrease the energy spread of the train induced by the beam loading.

First, the fields in the couplers are simulated and commented. A model for a whole HCS section (couplers and cells) is deduced and tested. Then, the introduction in PARMELA of bunch phase and beam loading is discussed.

III.1 Input and Output couplers

One major difficulty is to know if the HCS coupler fields are of travelling wave type, standing wave type or the superposition of the two types and in witch proportion. To answer this, the fields in the HCS couplers were calculated by the means of 3D HFSS program [5]. To save time, only the two couplers coupled by their axial iris are simulated (see figure 2). The diameter of the cylindrical apertures between wave guide and cavity-coupler was adjusted to obtain both a maximum transmission and a phase advance of $11\pi/12$ between the couplers at the operating frequency.

The amplitude and phase variations of the three field components E_z, E_r, B_φ along a path r=5mm are shown on schemas 3.a and b. The E_z and B_φ phases are constant and shifted of 90° all along the cavity-coupler except in the central part of the iris. Thus, this demonstrates the presence of a pure standing wave in the cavity. On the contrary, the small variation of E_r phase $\Delta\varphi=\pm7.5°$ inside the iris indicates that the travelling wave appears only over 1cm of the 2cm thick iris. In these conditions, the input and output $11\pi/12$ HCS couplers can be described in PARMELA program as fully standing wave cavities neglecting the small phase shift in the iris. We can notice that in the case of a mode further away from π, as usual $2\pi/3$ mode, the travelling wave spreads over all the iris, $\Delta\varphi$ increases to ±30° and the travelling wave becomes relatively more important.

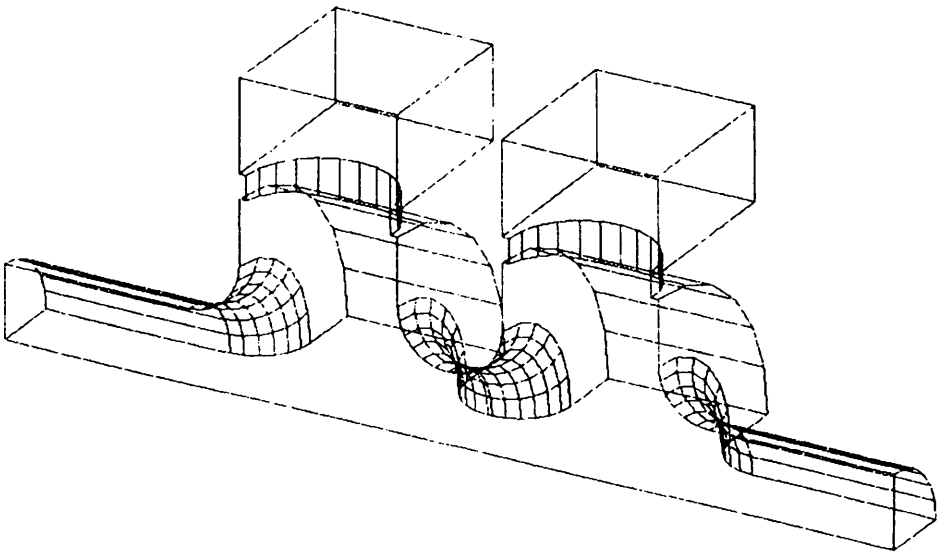

Figure 2: *HFSS mesh of the two HCS couplers. Thanks to the geometric and electromagnetic symmetries only the upper-left quarter is described with about 6000 tetrahedra. The cylindrical aperture between wave guide and cavity has a diameter of about 27mm. The input coupler is filled by a 2 Watt perfectly adapted source and the output coupler is terminated by an ideal unreflecting load.*

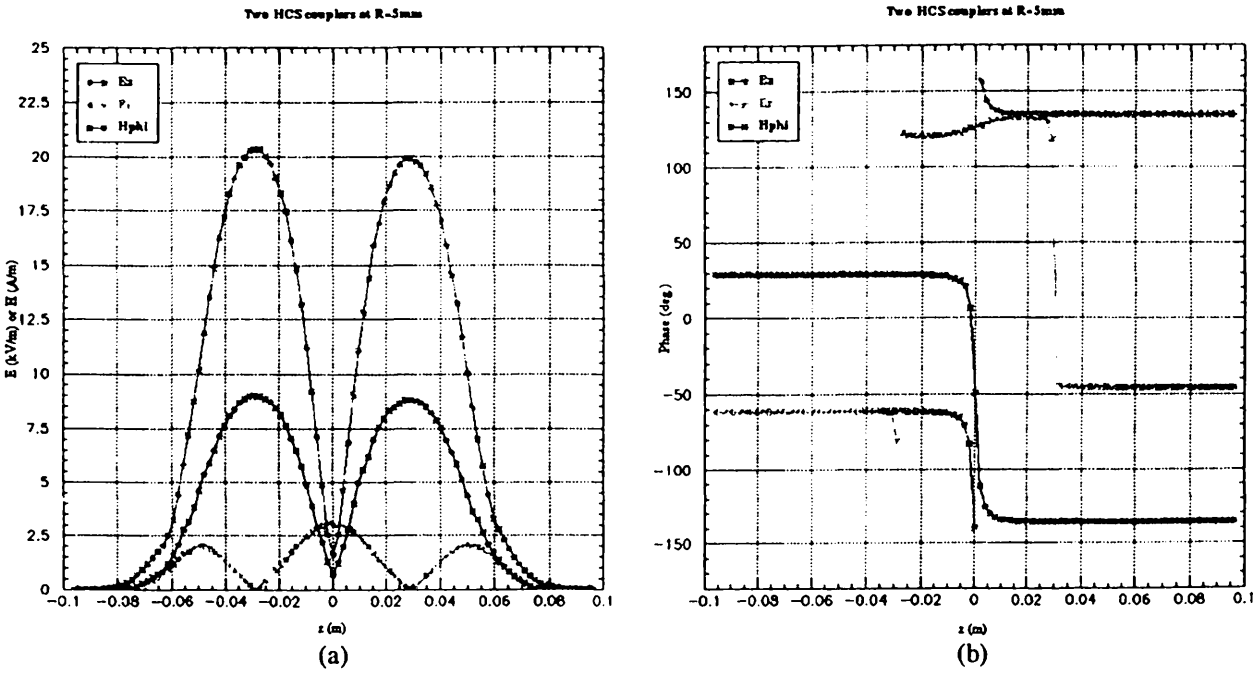

Figure 3: *Amplitude (a) and phase (b) variations of the E_z, E_r and H_φ fields with the axial position z in the two HCS couplers on 11π/12 operating mode.*

Finally, to give the shape of the coupler fields to PARMELA, the resonant π mode in the coupler cavity was calculated with SUPERFISH program. The fields are described in a data file readable by PARMELA with a table of E_z, E_r and B_φ function of z and r coordinates. This method allows to consider non-linearities in r direction and above all prevents from possible divergence of Fourier series when r increases (if description by Fourier coefficients rather than data file is chosen in PARMELA). The model of E_z along z axis calculated by SUPERFISH is drawn on figure 4. A cut-off tube of 5cm length is included in the coupler geometry to take care of fringe fields which reach 30% of the axial E_z maximum at the end of the cavity where the tube begins (point C).

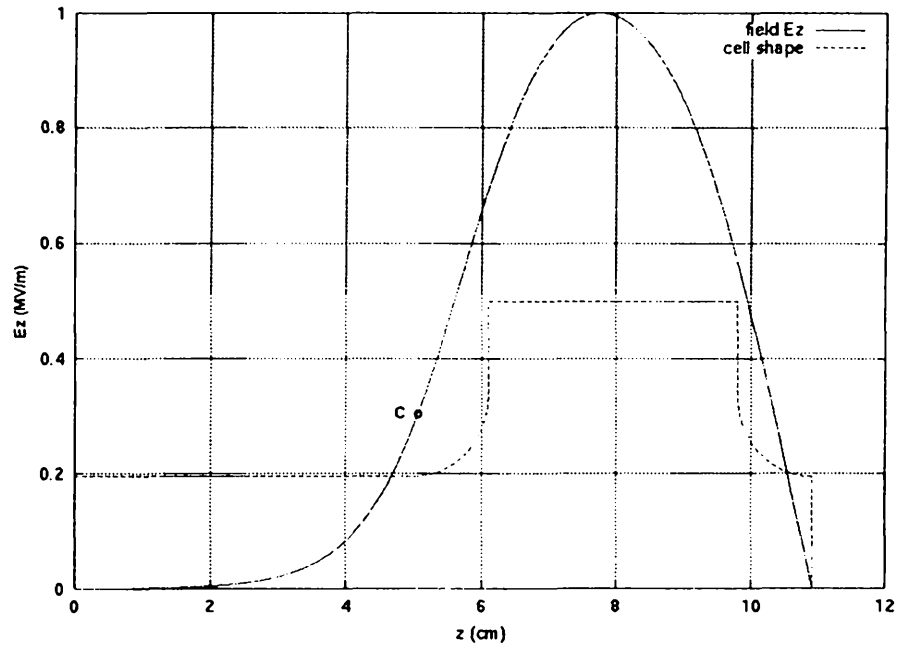

Figure 4: *Module of E_z field on the axis of the HCS cavity-coupler with 5cm cut-off simulated by SUPERFISH.*

III.2 The HCS sections: cells and couplers

After the study of the HCS couplers, the description of the whole section in PARMELA is explained and tested.

As the section is a travelling wave structure, the 13 cells between the couplers are described by the PARMELA travelling wave model with a $11\pi/12$ phase shift par cell. The HCS1 and HCS2 sections have also different frequencies. Thus, their cavities are simulated with their own frequencies of 3006.36MHz and 2998.74MHz and their cell lengths of 4.570cm and 4.594cm respectively. The attenuation along the travelling wave cells is not introduced cell to cell but the field amplitude of the cavities is uniformly set to the experimental average value.

In front of and behind these 13 cells are described the HCS couplers with two standing wave cells as explained before. According to the E_z field variations on axis measured by the "bead pulling" method in the HCS structures [6] [7], the amplitude of the input coupler is set to 1.5 from the average amplitude of the cells, the output coupler amplitude to 0.9. With these choices of magnitude, the experimental over-voltage of the couplers with respect to their neighbour cells is verified and only transformed in reference of the average cell amplitude. Then the phase advance between the coupler and the middle of next cell is set to 165° because of the operating HCS mode $11\pi/12$ verified by field measurements.

This model of HCS structure is used in PARMELA, and the field seen by a single axial ultra-relativistic electron travelling in phase with the HCS1 section is shown on figure 5. We can notice the E_z continuity along the z axis because the transformation between the travelling and standing wave occurs in the iris where field is nearly null.

To test the HCS model, comparisons of particle trajectories in HCS structure calculated with PARMELA and an other program RFSIM [8] were done. RFSIM written by R. Bossart is a code that resolves numerically the beam envelope equations in different electromagnetic elements and here in a HCS-like section with 13 standing waves cells. For example, with both PARMELA and RFSIM, a single electron at γ=14, r=10mm and r'=0 at the input is simulated in the HCS models with an average accelerating gradient of 35MV/m (no over-voltage is assumed here). Figure 6 shows the compared evolution of the transverse coordinates of the particle. In the two cases, the electron is strongly focused from r=10mm to 2mm. The trajectory differences are not larger than 0.4mm and 0.4mrad at the structure exit. This good agreement and others not presented here confirm the validity of the presented modelisation of the HCS sections in PARMELA.

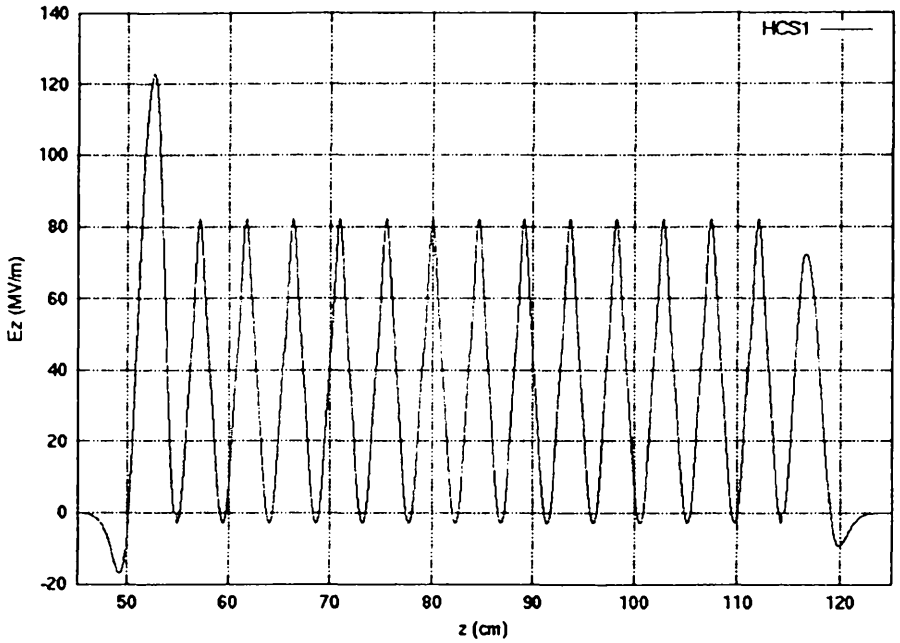

Figure 5: *E_z field seen by an ultra-relativistic particle on RF crest along the HCS1 axis*

III.3 Phase and beam loading of the bunches in HCS sections

Finally, the introduction of the bunch phase and the beam loading effects in the HCS structure are exposed in the PARMELA context.

The HCS frequencies are different of $\Delta f = \pm 7.81$MHz from the bunch frequency f_b=2998.55MHz. Therefore, the bunch phase in reference of the HCS RF crest moves slowly from the phase of the first bunch Φ_0 to the phase of the n^{th} bunch $\Phi_0 + 2\pi(n-1)\Delta f/f_b = \Phi_0 \pm (n-1)0.94°$. If the phase Φ_0 of the first bunch is -60° and +25° respectively for HCS1 and HCS2 as in the following simulations, the 24^{th} bunch will have an increased HCS1 phase of -22.5° and a decreased HCS2 phase of -12.5°. For the 48^{th} bunch, the phase reaches -16° for HCS1 and -19° for HCS2. This calculation has been done assuming that, at the location of the two sections, the bunch repetition is still exactly 2998.55MHz as at the time of the electron generation on the photo-cathode. In fact, from the photo-cathode to the HCS structures, the time spacing between each bunch slightly increases. To consider this phenomena in PARMELA simulations, the phases of HCS1 and 2 are first determined to have -60° and +25° at the passage of the first bunch. Then they are kept constant for the other bunches whereas the time of the bunch generation at the input of the PARMELA line is increased by 23 or 47 periods for the 24^{th} or 48^{th} bunch respectively.

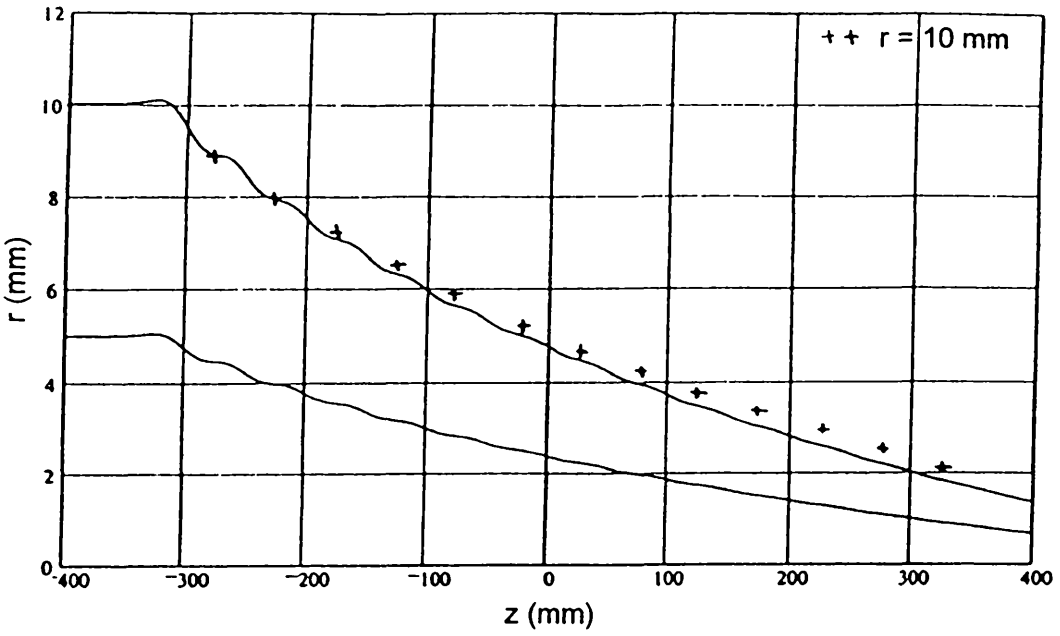

(a)

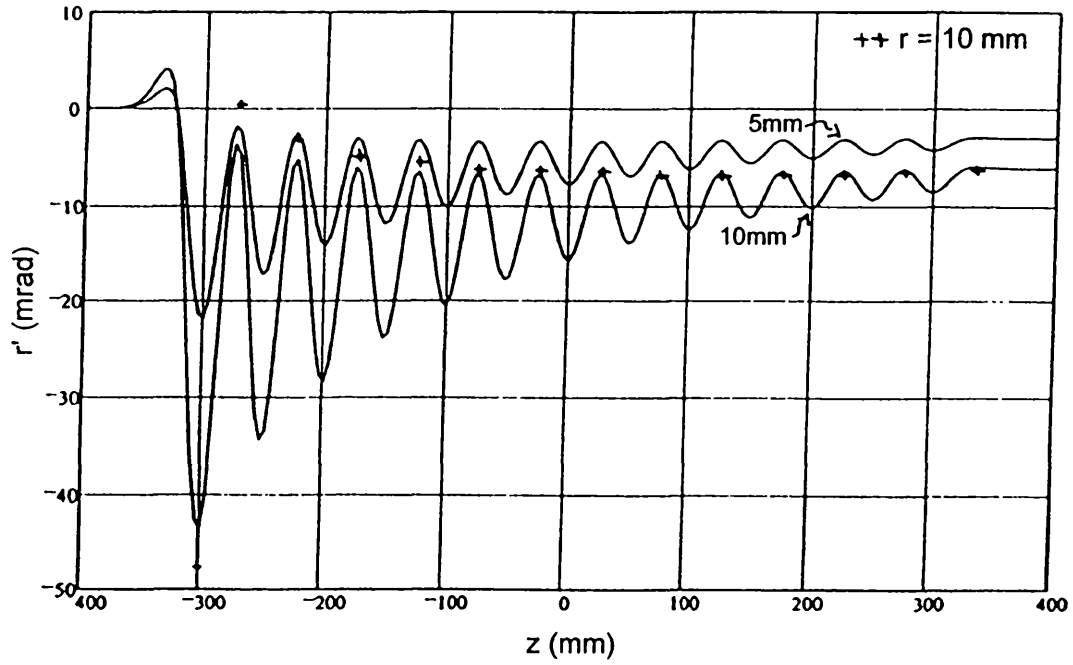

(b)

Figure 6: *Variations of the position (a) and divergence (b) of an uncentred single particle along one HCS-like structure simulated by both PARMELA and RFSIM program. The RFSIM results are drawn with solid lines for the two cases 10mm and 5mm, the PARMELA results are drawn with crosses for the case 10mm.*

With the beam loading in the sections, the energy gain ΔE can be evaluated [9] [10] for each bunch and section in function of the HCS frequency, the bunch charge Q_b=10nC and the beam loading factor $k_l = 6.76.10^{-3}$ MV/nC. For instance, the following expression may be used for the n^{th} bunch when the modification of the repetition rate in the line is neglected:

$$\Delta E_n = E_{av} \cdot L \cdot \cos\left[\phi_o + 2\cdot\pi\cdot(n-1)\cdot\frac{\Delta f}{f_b}\right] - 2\cdot Q_b \cdot k_l \cdot \left[\frac{1}{2} + \sum_{j=2}^{n} \cos\left[2\cdot\pi\cdot(j-1)\cdot\frac{\Delta f}{f_b}\right]\right]$$

It is not possible to introduce directly this value ΔE_n in the PARMELA input. But for each bunch n and section, the average accelerating gradient $V_{av\,n}$ is given according to the formula $V_{av\,n} = \Delta E_n / L / \cos(\Phi_0 + 2\pi(n-1)\Delta f / f_b)$ so that the bunch energy gain calculated in PARMELA reproduces the previous value ΔE_n. For HCS1 and HCS2, we find respectively the new gradients $V_{av\,n}$ equal to 34.8 and 34.9MV/m for the 1st bunch, 29.2 and 30.4MV/m for the 24th bunch and 26.4 and 26.3MV/m for the last bunch when the phase of the first bunch Φ_0 is still -60° and +25° of HCS RF crest.

IV. Inputs for the standing wave structures and magnetic elements

After the HCS sections, the other more classical components of the PARMELA lines are here quickly introduced.

The first and second solenoids are characterised by their constant field B_z of 0.3T and 0.1T along their effective length of 5.3cm and 7.7cm respectively. The motions of the macro-particles are simulated in the transverse and longitudinal plans.

The three quadrupoles of the triplet are ideally characterised by their magnetic gradient (see table 2 for their intensity) and their effective length 22.0cm. The B_x and B_y fields are then only described in first order of x or y variables, as the associated equations of motion.

Finally, for the booster run, the 2 cell booster and 5 cell buncher are described as fully standing wave sections operating in the π mode. Their electromagnetic fields E_z, E_r and B_φ were calculated with SUPERFISH and the results were introduced in PARMELA by means of a data file as for the cells of the HCS couplers. The fringe fields are considered over 5cm and the shape of the E_z component along z axis is drawn on figure 7 and 8. Their beam loading is classically calculated and introduced by the intermediate of their average accelerating gradient.

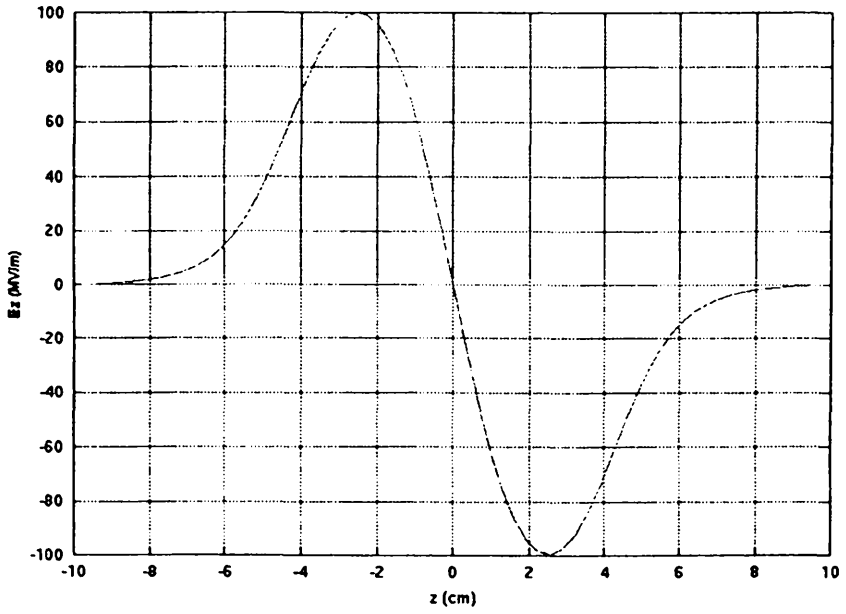

Figure 7: *Module of E_z field on the axis of the booster section with 5cm cut-off simulated by SUPERFISH.*

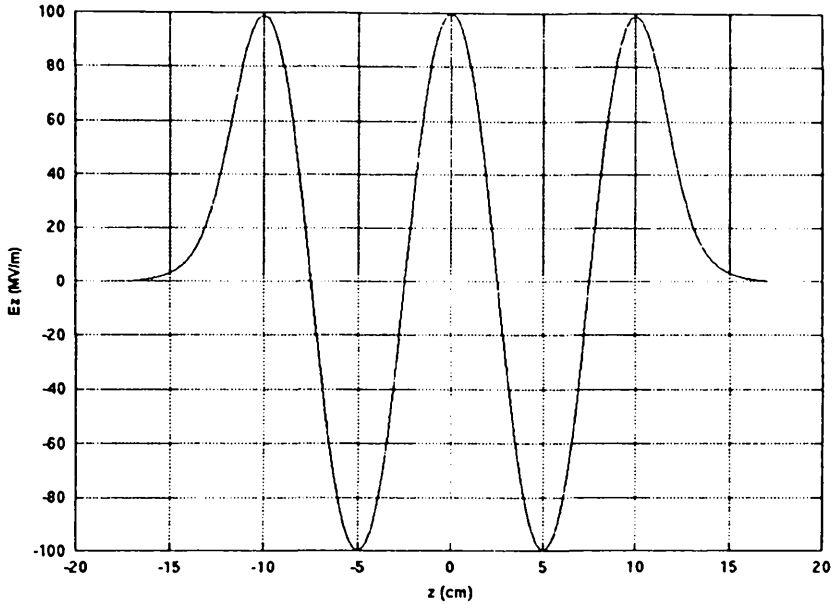

Figure 8: *Module of E_z field on the axis of the buncher section with 5cm cut-off simulated by SUPERFISH.*

V. Two different PARMELA runs

In the previous paragraphs, the different elements of the two layouts considered were described: their main characteristics were given and how they are introduced in PARMELA runs. Now, the emphasis is put on the results of the simulations and their discussion. Numerous runs were done to study the RF properties and beam transmission through the first elements of the CTF2 drive beam. Here, only two cases are reported and discussed. Their choice allows to reveal some interesting RF beam dynamic properties and to compare the two different layouts.

As seen before (figure 9 and table 2), these cases both involve the gun4, solenoid 1, the HCS structures and the first triplet. They differ by the presence of either a second solenoid or a booster just before the accelerating sections and the addition of a buncher after the triplet in the second case only.

Some results of these two PARMELA simulations for the three bunches n° 1, 24, 48 are presented and summarised in figures 11 - 14 and tables 3 - 4. First, the figures 11 and 12 show the x and y trajectory of a single electron which is generated at the input of PARMELA run with maximum coordinates for (x, x') and (y, y'), see table 1. This particle is then tracked along the line (without space charge because single). Its trajectory does not give the exact beam envelope but allows to have good understanding of the focusing effects in the different elements and easily reveals the presence and the approximated location of the maxima and waists in x or y plans. Secondly, the figures 13 and 14 come from the tracking of 1000 macro-particles with space charge calculation. We can find the graphical evolution of the rms values of x, x', y, y', bunch energy spread and transmission along the axis. The corresponding tables 3 and 4 give rms numerical values to the beam characteristics Δz, $\Delta\gamma/\gamma$, x, x', the average energy γ and the rms normalised emittance ε_x for a choice of z positions. So, in the following text, the beam dynamics will be analysed and compared between the two runs.

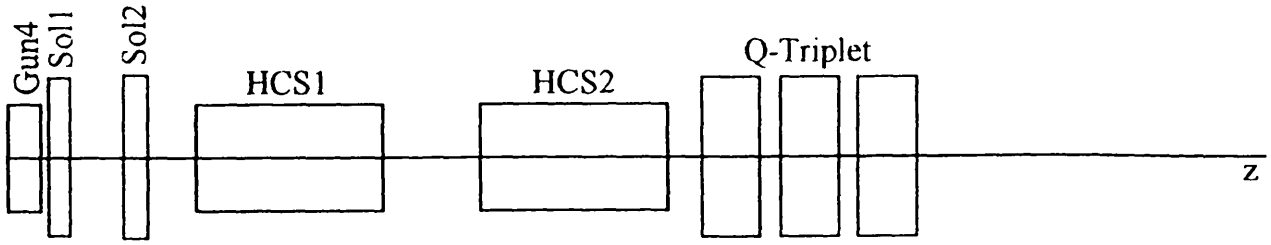

(a) Nov 98 configuration

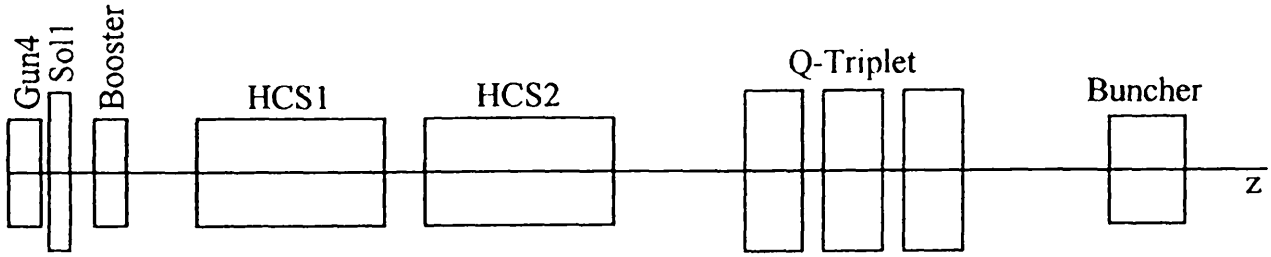

(b) Booster configuration

Figure 9: *Schematic layout of the CTF2 components for the two simulated lines.*

	Nov 98 layout			Booster layout		
		z-Position *	Settings		z-Position *	Settings
Photo-cathode	†	0.0cm	Ølaser 11mm	†	0.0cm	Ølaser 11mm
Gun 4	†	5.6cm	100MV/m laser 30° of RF crest	†	5.6cm	100MV/m laser 30° of RF crest
Solenoid 1		17.4cm	3100G	†	17.4cm	3000G
Solenoid 2		47.4cm	1170G		/	/
Booster		/	/		38.4cm	35MV/m 0° of RF crest
HCS1 section		75.0cm	35MV/m -60° of RF crest		75.0cm	35MV/m -60° of RF crest
HCS2 section		181.5cm	35MV/m +25° of RF crest		159.8cm	35MV/m +25° of RF crest
QFN 130		270.0cm	84G/cm		286.4cm	105G/cm
QFN 131		299.8cm	167G/cm		316.3cm	210G/cm
QFN132		329.6cm	104G/cm		346.1cm	130G/cm
Buncher		/	/		426.5cm	35MV/m -45° of RF crest
Out PARMELA		464.8cm	/		463.7cm	/
Z=0 PARMELA		2.4cm	/		27.4cm	/

Table 2: *Position and settings of the components for the 2 simulated lines. * The positions are given from the photo-cathode to the middle of the element except for the HCS1 and HCS2 sections where the reference is the middle of the input wave guide. In the booster configuration, the HCS2 section and the triplet are slightly moved to allow the addition of the 'idler cavity' between them in the test facility. † The corresponding element is not integrated in the PARMELA simulation.*

V.1 Two solenoids or solenoid-booster configuration

First, with the booster configuration, the maxima of the transverse sizes x, y of the beam are smaller by 20% than with the two solenoid configuration. The maximum radius are of 10.4mm and 13.0mm.

Further, at the entrance of HCS1, the three bunch trajectories of the Nov 98 configuration are really more separated in radius and divergence than with the booster. Beam radius and divergence are also larger for the two solenoids. For comparison, the x=y rms value moves from 5.6±0.1mm to 6.4±0.3mm and the x'=y' rms divergence from 2.80±0.4mrad to 3.35±1.7mrad for booster and Nov 98 layouts respectively.

Of course, the booster gives a supplementary energy to the bunches. The gain is of 3.4MeV to 2.8MeV for the first and 48th bunch assuming the booster beam loading. The energy spread between the bunches is slightly increased from 0.48MeV of the gun4 to 0.78MeV, but the intra-bunch energy spread stays constant with less than 0.12MeV rms.

And the booster increases the bunch normalised emittance $\varepsilon_x=\varepsilon_y$ with a variation of +7mm.mrad compared to +2mm.mrad with the two solenoid solution. With a tracking realised here with 1000 particles, the relative numerical error on ε is of a few mm.mrad, the variation due to booster is nearly within this error and thus is very low. If the emittance blow-up by the input coupler of HCS1 is considered also, the total emittance blow-up after the HCS1 coupler is larger for the configuration with two solenoids than for the booster case.

V.2 HCS1 and HCS2 sections

When a particle arrives and travels through the HCS sections, it sees electromagnetic fields depending on the relative phase between the particle and the RF crest of the section. On figure 9, the E_z component seen by the reference axial particle of the 1st, 24th and 48th bunch is drawn along HCS1 and HCS2.

The E_z field in the HCS1 input coupler presents a negative decelerating part in the fringe field region which reaches -56MV/m for the 1st bunch with the biggest phase shift -60°, -33MV/m for the 24th bunch at -22.5° and -17MV/m for the last bunch at -15° of RF crest. This deceleration and field shape induce strong focusing force in the coupler proportionally to the bunch phase shift. For instance, a particle of the 1st bunch arriving with x=10mm and x'=3.8mrad will be focused and go out from the coupler with still x=10mm but x'=-3.8mrad.

For the input coupler of HCS2, the fringe fields reach -17MV/m and defocusing occurs again but really with less magnitude because the particles have already gained more than 10MeV in the HCS1 section and are more rigid.

For the HCS1 output coupler, the field seen by the particles in the cut-off region is really small, less than -4MV/m and no focusing effect is observed.

For the HCS2 section, according to the different phase, the fringe fields of the output coupler are larger than for HCS1. A defocusing effect is observed but very slight because of the yet high energy of 45MeV.

So, focusing and defocusing forces are put in evidence in input and output HCS couplers respectively. Their amplitude depends on the accelerating gradient, bunch phase and particle energy. The dominant effect however is the focusing of the HCS1 input coupler.

The strong focusing of the HCS1 input coupler gives big kicks to the particles and the rms normalised emittance increases in the coupler to about 126mm.mrad instead of 62mm.mrad just at the HCS1 input. But this variation will be progressively compensated by the low focusing of the two travelling wave sections.

An other consequence of the HCS input focusing is the formation of an x and y waist at short distance z where the particles cross the beam axis. According to the beam characteristics at the HCS1 input, the waist is located approximately between the 2 sections for the Nov 98 configuration and can be pushed downstream after the two sections into the triplet for the booster configuration. We may notice that the space charge effects further move the waist by about 25-30cm, move which can be compensated by an adjustment of the solenoid.

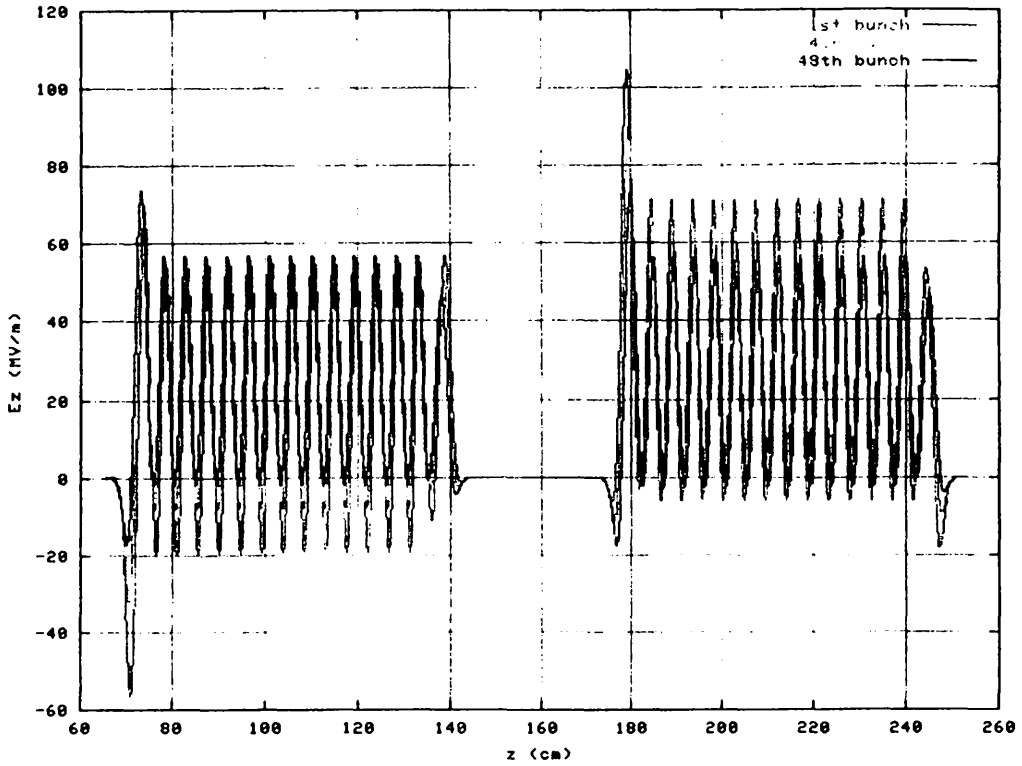

Figure 10: *E_z field seen by the reference particle on HCS1 and HCS2 axis. The first bunch arrives at -60° and +25° of the RF crest of HCS1 and HCS2 respectively.*

Exit of HCS2 section

At the exit of HCS2 (or input triplet), the beam is characterised in size, energy and emittance and the two runs are compared.

The radius of the beam for the booster layout is significantly lower than for the 2 solenoid line. It decreases by 20% from 1.5±0.3mm to 1.2±0.1mm rms for the booster. At the same time, the divergence decreases also by 30% from 2.4±0.2mrad divergent to 1.6±0.15mrad rms convergent.

About the energy, we may remark that at the HCS2 exit the average energies of the first and 48th bunches are almost identical and the lowest ones whereas the 24th bunch presents the biggest energy. As example, for the booster case, the average energies are respectively 44.8MeV, 47.2MeV and 44.4MeV. Thus, the energy spread of the train is of ±1.40MeV. For the intra-bunch energy spread (fig. 13-14 T_{kin}), the HCS1 phase shift -60° of the 1st bunch induces a ΔE_{rms} up to ±1.25MeV at the HCS1 end that is compensated later by the second HCS2 section at +25°. At the HCS2 exit, the rms intra-bunch energy spread of the bunches is only of ±0.66MeV for booster line or ±0.59MeV for Nov 98 line. Thus, the demonstration has been done that the beam loading compensation scheme is well simulated by PARMELA: the average bunch energy spread is compensated by HCS1 and HCS2 as well as the intra-bunch energy spread at the chosen bunch phase.

The particle transmission through both HCS is total and the HCS2 exit emittance is almost identical to the HCS1 input value in spite of the quick growth in the first HCS1 coupler. The rms ε magnitude is of about 72mm.mrad for the booster line and 69mm.mrad for the two solenoid line.

V.3 First quadrupole triplet

Evidently, the triplet allows to maintain the transverse sizes of the beam from HCS2 output. Moreover, it focuses the already strongly divergent beam of the Nov 98 configuration from more than 2.4mrad rms to 0.9mrad rms. At the line output, about 465 cm from the photo-cathode, the beam envelope has a maximum extension of 8mm and is unsymmetric in horizontal and vertical plans whereas it is lower than 4mm and symmetric for the booster configuration. We may notice that the experimental settings of the triplet were used in the 2 solenoid case, but not in the booster run. Variations of less than 10% of the quadrupole currents do allow to obtain more cylindrical beam but no significant smaller radius in Nov 98 case. Optimisation of triplet requires tracking further down the whole 3 GHz line till the entrance of the transfer structures and this is the subject of another analysis.

V.4 Buncher element

For the booster configuration, the insertion of a 5 cell buncher after the triplet does not change the transverse trajectories x, y neither the emittance because of the already high particle energy of 45MeV. By choosing the RF phase, the buncher has the advantage to modify easily the intra-bunch energy spread necessary to the magnetic bunch compressor, independently of the settings of the HCS phases. Here, the buncher phase of -45° increases the intra-bunch energy spread of 50% with a new rms value ±1.1MeV instead of ±0.7MeV. Simultaneously, the average energy is increased up to 50.0±2.0 MeV and the buncher beam loading must be compensated by the HCS phasing.

VI. Conclusion

The use of PARMELA program to simulate the first elements of the CTF2 drive beam provides a good understanding of beam generation and transformation from MAFIA cylindrical results to PARMELA cartesian description with equal charge density.

Secondly, a PARMELA model for the HCS travelling wave section of $11\pi/12$ mode was determined. The use of a fully standing wave cell for the couplers was justified by independent HFSS simulations and the new model was validated by comparisons with the RFSIM beam envelope program.

In the HCS sections, RF effects on beam dynamics were demonstrated. The input couplers are focusing and the output couplers are defocusing in principle. In fact, the focusing magnitude depends mainly on bunch phases, HCS gradients and particle energies. In CTF2, the input coupler of HCS1 has significant implications and is the most critical component which induces strong focusing, local emittance growth, short-distance x and y waists and a divergent beam at the HCS2 output in the Nov 98 configuration. It must be noted that PARMELA does not deal with wakefields so that possible effects of these fields in HCS are under investigation in a different way.

The PARMELA simulations and comparisons of the two layouts present a total transmission until 450cm from the gun4 photo-cathode for a charge of 10nC per bunch and a laser spot diameter of 11mm. It was demonstrated that the booster allows to increase the average energy and to obtain a better beam envelope at the exit of HCS2 with a radius diminution from 1.7 to 1.2mm rms and a divergence diminution from 2.4 (divergent) to -1.6 (convergent) mrad rms compared to the Nov 98 configuration. Whereas, the energy spread and emittance do not change significantly. Furthermore, a standing wave buncher after the triplet was proposed to induce supplementary phase-energy correlation and average energy in the line.

In the future, the installation of the booster section in the CTF2 test facility instead of the second solenoid will improve the beam radius and the beam divergence. On the other hand, from current PARMELA inputs, the study of the drive beam transport will be enlarged to the entrance of the 30 GHz transfer structures and will include all quadrupole triplets and the magnetic bunch compressor to simulate, compare and try to ameliorate the understanding of the experimental measurements and transmission in the 30 GHz sections.

Acknowledgements

Many thanks to the CTF team and especially to G. Guignard, A. Riche and M. Valentini for their advice. I also want to express my gratitude to R. Bossart for all the common work, constructive discussions and numerous RFSIM comparative simulations. And I do not wish to forget B. Mouton and Y. Thiery (LAL, Orsay) for their expertise and help on unix SUPERFISH and PARMELA simulations.

References

[1] "The CLIC test facility: CTF2 a Two-Beam Test Accelerator for Linear Collider Studies", CTF2 design report, CLIC Team, CERN/PS/96-14 (LP), June 96

[2] "The PARMELA Program", B. Mouton, LAL/SERA 93-455, Sep 93

[3] "MAFIA Simulations on Gun 4", M. Dehler, Private Communication, 97

[4] "A High Current, High Gradient Electron Double Accelerating structure", J. Bienvenu and J. Gao, EPAC96, 10-14 June 96

[5] "Maxwell, Eminence User's reference", Ansoft corporation, May 95

[6] "RF Measurements on Accelerating structure HCS1", R. Bossart and M. Chanudet, CERN PS/RF/Note 97-14, Sept 97

[7] "RF Measurements and tuning of the accelerating section HCS2", R. Bossart and M. Chanudet, CERN PS/RF/Note 98-04, Feb 98

[8] "On program RFSIM solving the beam envelope equation", R. Bossart, Private communication, Feb 97

[9] "Analytical Calculation of Beamloading Compensation in the High Charge Structures", M. Valentini and H. Braun, CERN PS/LP CTF Note 98-05, Feb 98

[10] "Beamloading calculation for the HCS section", R. Bossart, Private communication, 98-99

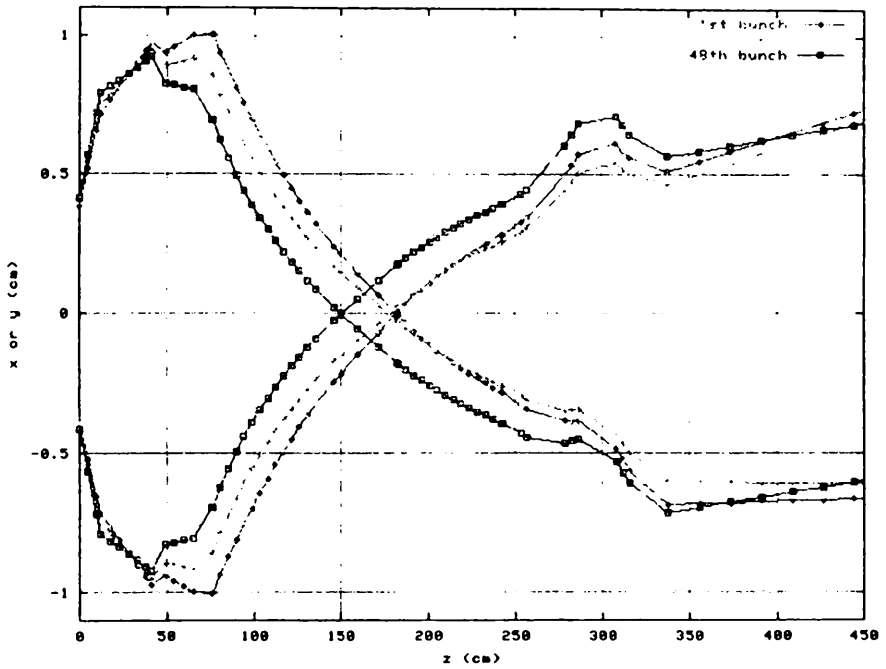

Figure 11: *X and y trajectories along the Nov 98 layout of the outer most particle of the PARMELA beam generation.*

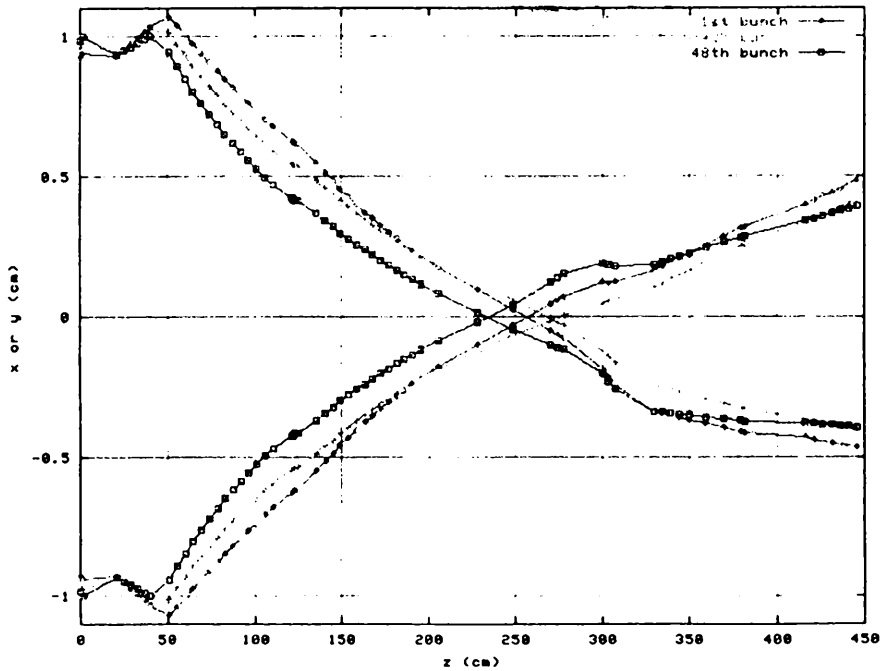

Figure 12: *X and y trajectories along the booster layout of the outer most particle of the PARMELA beam generation.*

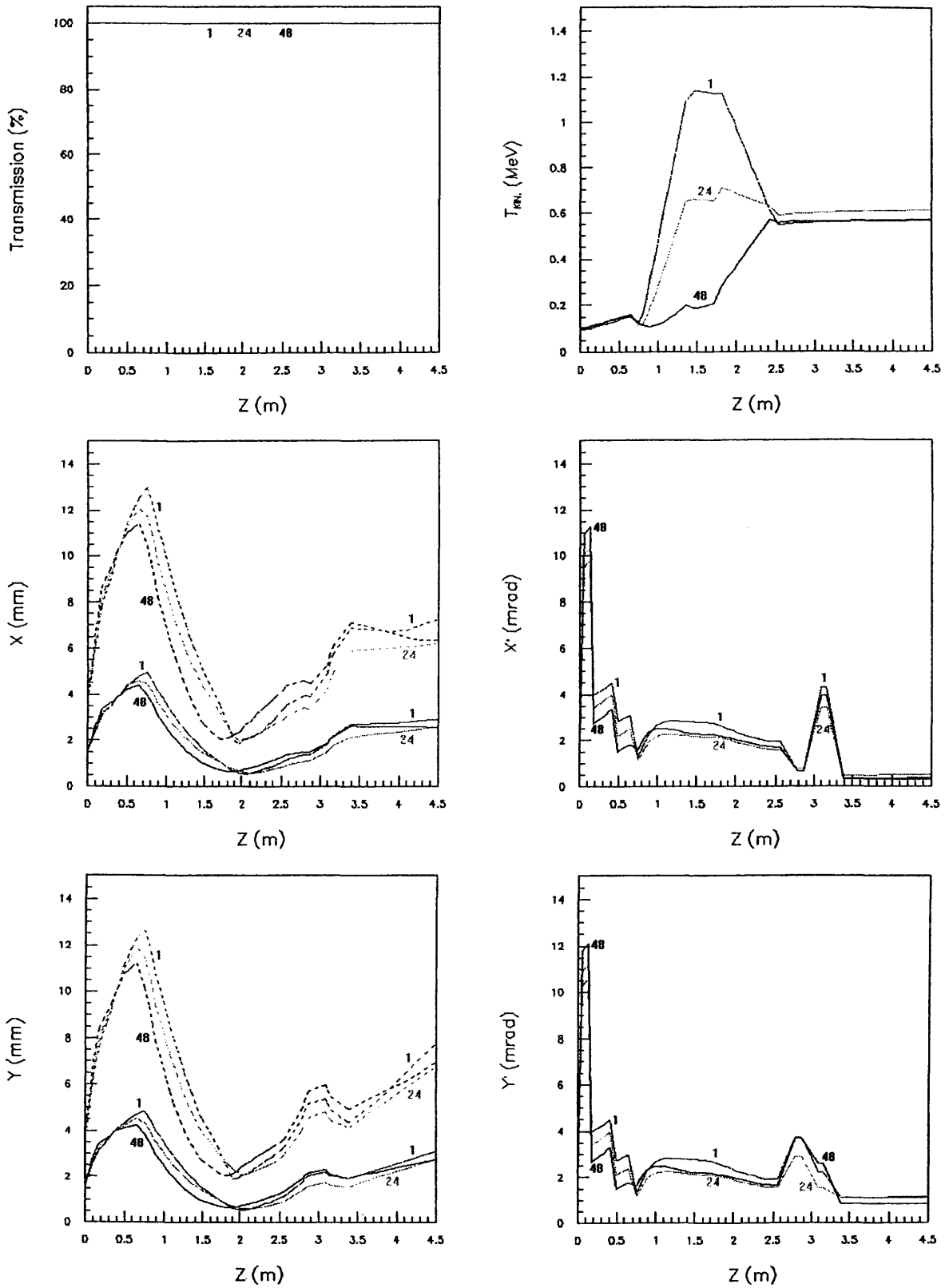

Figure 13: *Transmission, intra-bunch energy spread, x, x', y and y' variations along the Nov 98 layout simulated with 1000 macro-particles. The numbers 1, 24 and 48 (and the red, green and blue colours) refer to the 1st, 24th and 48th bunches respectively. Rms values are drawn by solid lines, maxima by dashed lines.*

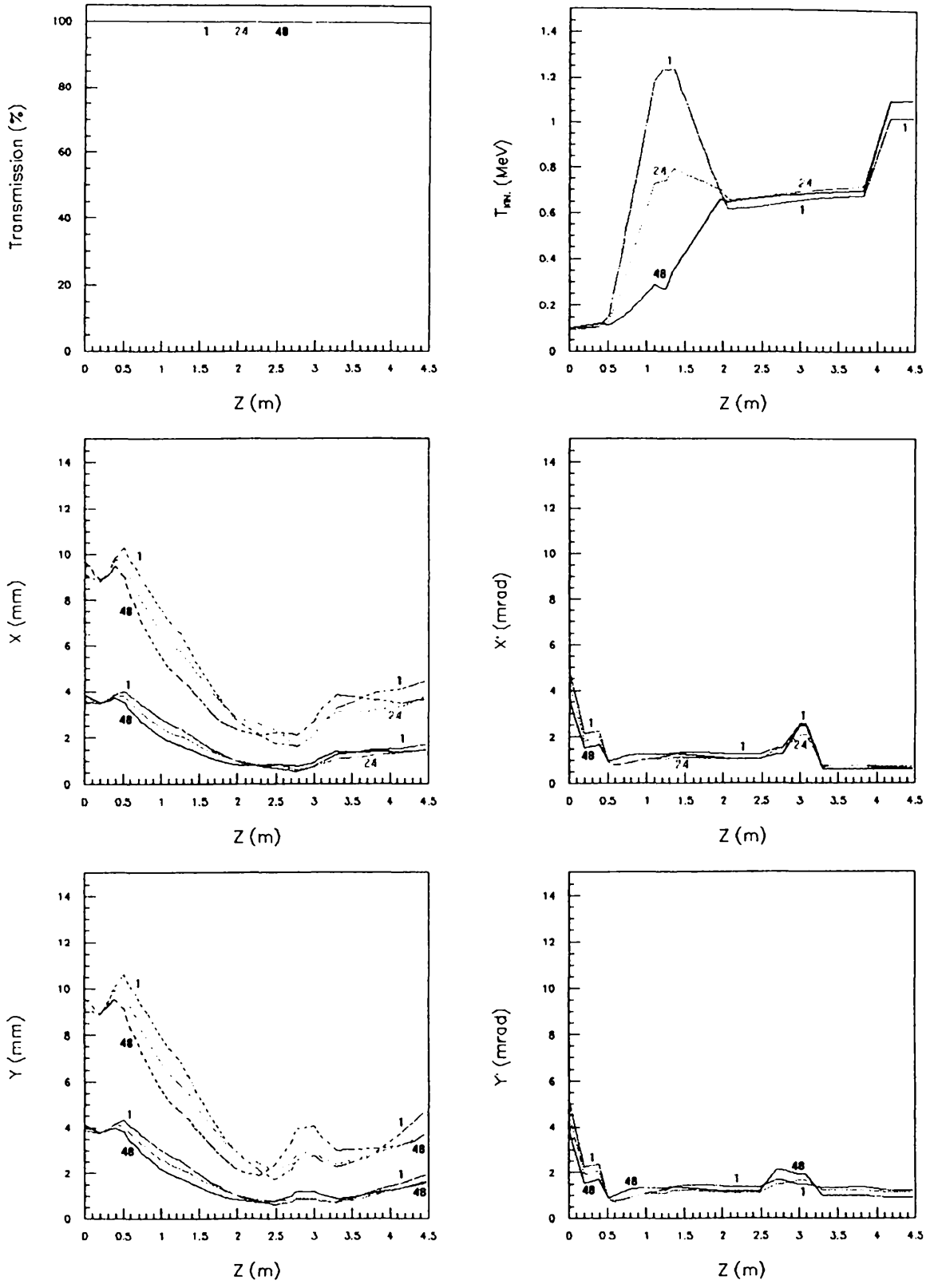

Figure 14: *Transmission, intra-bunch energy spread, x, x', y and y' variations along the booster layout simulated with 1000 macro-particles. The numbers 1, 24 and 48 (and the red, green and blue colours) refer to the 1st, 24th and 48th bunches respectively. Rms values are drawn by solid lines, maxima by dashed lines.*

HCS1 at 3006.36MHz:	**1st bunch,**	**34.8MV/m,**	**-60.0° of rf crest**	**Beam data for GUN4 with Virtual cathode.**
	24th bunch,	29.2MV/m,	-37.5° of rf crest	**Photo-cathode diameter 11mm, 10nC per bunch,**
	48th bunch,	26.4MV/m,	-15.0° of rf crest	2998.55MHz repetition rate
HCS2 at 2990.74MHz:	**1st bunch,**	**34.9MV/m,**	**+25.0° of rf crest**	
	24th bunch,	30.4MV/m,	2.5° of rf crest	**Magnetic element settings:**
	48th bunch,	26.3MV/m,	-20.0° of rf crest	SNF100: 3100G SNF110: 1170G
				QFN130: 84.0G/cm QFN131: -167.0G/cm QFN132: 104.0G/cm

	no bunch	Virtual cathode	in Sol1	in Sol2	in hcs1	out cp1 hcs1	in cp2 hcs1	out hcs1/ in hcs2	out cp1 hcs2	in cp2 hcs2	out hcs2/ in triplet	out triplet	out line
z cm		0.0	10.2	37.8	65.0	75.9	135.4	159.8	182.4	242.2	253.1	338.4	462.6
Trans.	1	100.	100.	100.	100.	100.	100.	100.	100.	100.	100.	100.	100.
%	24	100.	100.	100.	100.	100.	100.	100.	100.	100.	100.	100.	100.
	48	100.	100.	100.	100.	100.	100.	100.	100.	100.	100.	100.	100.
σ_z	1	.9893	.9879	.9933	1.0088	1.0155	.9706	.9529	.9394	.9393	.9393	.9393	.9393
mm	24	1.0179	1.0166	1.0244	1.0453	1.0520	1.0444	1.0444	1.0444	1.0444	1.0444	1.0444	1.0444
	48	1.0473	1.0462	1.0576	1.0861	1.0953	1.0907	1.0907	1.0907	1.0907	1.0907	1.0907	1.0907
γ	1	14.005	14.049	14.087	14.104	14.467	35.263	37.907	43.266	79.336	81.183	81.262	81.292
	24	13.105	13.148	13.181	13.195	15.157	42.193	44.764	49.112	84.282	86.606	86.681	86.716
	48	12.105	12.148	12.176	12.185	15.260	44.944	47.215	50.171	79.699	82.045	82.097	82.114
σ_γ/γ	1	1.3386	1.3822	1.7038	2.0590	1.7374	6.0562	5.8348	5.0666	1.5070	1.3181	1.3468	1.3583
%	24	1.5145	1.5584	1.9018	2.2950	1.4447	3.0128	2.8706	2.8364	1.4614	1.3309	1.3617	1.3804
	48	1.6962	1.7446	2.1226	2.5809	1.4967	.8564	.7963	1.1318	1.3932	1.3246	1.3422	1.3553
$<\sigma_x,\sigma_y>$	1	2.1637	3.5610	5.5275	6.7295	6.9494	2.8122	1.8406	1.1017	1.2947	1.5394	3.2428	4.3565
mm	24	2.2422	3.7187	5.5289	6.4637	6.2579	2.4558	1.7402	1.1957	1.0614	1.2346	2.6502	3.8757
	48	2.3214	3.9237	5.5303	6.1073	5.5473	1.7713	1.1512	.9136	1.6235	1.8321	3.1961	3.8332
$<\sigma_{x'},$	1	15.1135	14.2521	6.2402	4.2764	4.5488	3.9009	3.8759	3.7419	2.6861	2.6837	1.0416	1.0663
$\sigma_{y'}>$	24	15.9057	15.0644	5.5146	3.4235	2.3915	3.0654	3.0117	2.9448	2.2370	2.2192	1.1151	1.1382
mrad	48	17.1718	16.3773	4.5859	2.5201	1.9940	3.2632	3.1537	3.0340	2.3770	2.3425	.8218	.8356
$<\varepsilon_x, \varepsilon_y>$	1	48.11	57.94	60.35	62.11	126.29	73.65	71.20	70.26	69.26	69.38	69.47	70.09
mm.mrad	24	49.16	58.35	61.41	63.55	85.82	70.06	69.21	69.00	68.09	68.13	68.09	68.51
	48	51.22	59.99	64.11	66.38	70.12	69.70	69.65	69.44	69.21	69.18	69.27	69.87

Table 3: *Numerical values of the main beam characteristics along the Nov 98 layout simulated with 1000 macro-particles.*

Booster at **2998.55MHz:**	**1st bunch,**	**35.0MV/m,**	**0.0° of rf crest**
	24th bunch,	32.0MV/m,	0.0° of rf crest
	48th bunch,	29.0MV/m,	0.0° of rf crest
HCS1 at **3006.36MHz:**	**1st bunch,**	**34.8MV/m,**	**-60.0° of rf crest**
	24th bunch,	29.2MV/m,	-37.5° of rf crest
	48th bunch,	26.4MV/m,	-15.0° of rf crest
HCS2 at **2990.74MHz:**	**1st bunch,**	**34.9MV/m,**	**+25.0° of rf crest**
	24th bunch,	30.4MV/m,	2.5° of rf crest
	48th bunch,	26.3MV/m,	-20.0° of rf crest
Buncher at **2998.55MHz**	**1st bunch,**	**35.0MV/m,**	**-45° of rf crest**
	24th bunch,	32.3MV/m,	-52° of rf crest
	48th bunch,	29.9MV/m,	-60° of rf crest

Beam data for GUN4 and Solenoid at 0.300T
Photo-cathode diameter 11mm, 10nC per bunch,
2998.55MHz repetition rate

Magnetic element settings:
QFN130: 105G/cm QFN131: --210G/cm QFN132: 130G/cm

	no bunch	out gun in boo	in hcs1	out cp1 hcs1	in cp2 hcs1	out hcs1/ in hcs2	out cp1 hcs2	in cp2 hcs2	out hcs2/ in triplet	out triplet	in buncher	out buncher	out line
z cm		0.0	40.0	50.9	110.3	122.8	135.7	195.4	206.3	329.9	382.1	416.5	436.5
Trans. %	1	100.	100.	100.	100.	100.	100.	100.	100.	100.	100.	100.	100.
	24	100.	100.	100.	100.	100.	100.	100.	100.	100.	100.	100.	100.
	48	100.	100.	100.	100.	100.	100.	100.	100.	100.	100.	100.	100.
σ_z mm	1	.9893	.9916	.9905	.9649	.9518	.9501	.9501	.9501	.9501	.9501	.9501	.9501
	24	1.0179	1.0211	1.0207	1.0057	1.0055	1.0057	1.0057	1.0057	1.0057	1.0057	1.0057	1.0057
	48	1.0473	1.0523	1.0528	1.0495	1.0492	1.0495	1.0495	1.0495	1.0495	1.0495	1.0495	1.0495
γ	1	14.005	20.699	21.019	41.391	44.034	49.426	85.951	87.842	87.843	87.877	99.713	99.723
	24	13.105	19.220	21.133	47.849	50.431	54.756	89.998	92.342	92.330	92.357	101.82	101.83
	48	12.105	17.642	20.658	50.172	52.492	55.352	84.458	86.809	86.835	86.847	93.981	93.987
σ_γ/γ %	1	1.3386	1.0189	1.4927	5.5916	5.4746	4.8648	1.5765	1.3763	1.4886	1.5054	2.0012	2.0023
	24	1.5145	1.1611	1.2235	2.9775	2.8746	2.8428	1.5368	1.4037	1.4965	1.5218	2.1087	2.1109
	48	1.6962	1.3297	1.0762	1.1252	1.0141	1.2761	1.5345	1.4701	1.5538	1.5732	2.2811	2.2832
$<\sigma_x,\sigma_y>$ mm	1	5.1767	5.6929	5.9178	3.8445	3.5546	3.1685	1.4885	1.3152	1.4001	1.9318	2.2012	2.4296
	24	5.3705	5.6236	5.5791	3.3036	3.0703	2.7931	1.4849	1.3541	1.2530	1.6263	1.8830	2.0923
	48	5.5317	5.4702	5.1965	2.7082	2.4699	2.2309	1.1922	1.1130	1.6023	1.7840	1.9092	2.0379
$<\sigma_{x'},$ $\sigma_{y'}>$ mrad	1	7.5003	3.2828	3.7614	1.5682	1.6952	2.1980	1.8851	1.8430	1.4491	1.4647	1.3125	1.3162
	24	6.6847	2.8452	2.4333	1.4938	1.5266	1.7132	1.5429	1.5153	1.3725	1.3842	1.2832	1.2866
	48	5.7118	2.3986	1.4770	1.8199	1.7953	1.8181	1.6163	1.5949	1.1250	1.1321	1.0681	1.0711
$<\varepsilon_x, \varepsilon_y>$ mm.mrad	1	60.33	67.81	110.75	76.07	74.80	71.32	71.01	70.86	70.28	70.37	70.42	70.48
	24	62.33	69.95	88.77	75.53	74.69	73.73	73.20	73.10	72.58	72.68	72.51	72.49
	48	64.32	71.37	75.46	73.91	73.74	74.01	73.56	73.54	72.93	73.14	73.12	73.16

Table 4: *Numerical values of the main beam characteristics along the booster layout simulated with 1000 macro-particles.*